Electronic Supplementary Material (ESI) for Dalton Transactions.

Supporting Information

Tetranuclear Cobalt(II)-Isonicotinic Acid Frameworks: Selective CO_2 Capture, Magnetic Properties, and the Derived "Co_3O_4" Exhibiting High Performance on Lithium Ion Batteries

Lei Zhou, Honghong Fan, Baolei Zhou, Zheng Cui, Bowen Qin, Xiaoying Zhang*, Wenliang Li* and Jingping Zhang*

Advanced Energy Materials Research Center, Faculty of Chemistry, Northeast Normal University, Changchun 130024, P. R. China

Corresponding Author

* jpzhang@nenu.edu.cn

* zhangxy218@nenu.edu.cn

* liwl926@nenu.edu.cn

Electrode prepared. For the electrochemical measurements, the working electrode consisted of pristine Co_3O_4 active materials, electrical conductor acetylene black and binder PVDF (in a weight ratio of 70:15:15) on copper foil. For lithium ion batteries, pure lithium foil was used as the counter electrode and 1.0 M $LiPF_6$ dissolved in ethylene carbonate/dimethyl carbonate mixture (in a volume ratio of 1:1) as the electrolyte. The 2032 coin cells were assembled in an argon-filled glovebox.

Physical Measurements. Elemental analyses (C, H, N) were performed on an Elementar Vario EL analyze. TG analyses were performed on a NETZSCH STA 409PC instrument in flowing N_2 at a heating rate of 5°C·min^{-1} from room temperature to 800°C. X-ray powder diffractometry (PXRD) studies were performed on a Siemens D5005 diffractometer with Cu−Kα radiation (λ = 0.154 nm) in the range of 3−50° at room temperature. The magnetic measurements have been obtained with the use of a Quantum Design MPMSXL-5 SQUID instruments. Volumetric H_2 adsorption–desorption isotherms were measured at 77 K using an ASAP 2020 HD (Micromeritics). Volumetric CO_2 sorption isotherms were collected at 273 K and 298 K using an AutosorbIQ (Quantachrome Instruments). Volumetric N_2 sorption isotherms were collected at 77 K using an AutosorbIQ (Quantachrome Instruments). Volumetric CH_4 adsorption–desorption isotherms were measured at 273 K using 3Flex (Micromeritics). All electrochemical measurements were performed using a Land battery test system (LAND CT2001A) from 0.01 to 3 V. The morphology of sample was studied by transmission electron microscope (TEM, JEOL-2100F, 200 kV) and scanning electron microscope (SEM, (JEOL JSM-6700F field emission).

Single-Crystal X-ray Crystallography. The crystal data were collected on an Oxford Diffraction Gemini R Ultra detector diffractometer (Mo-Ka, graphite monochromator, λ = 0.071073 nm) at 298 K for compounds **1** and **2**. Suitable crystals were affixed to the end of a glass fiber using silicone grease and transferred to the goniostat. The structures were solved by the direct method and refined by the full-matrix least-squares method on F^2 using the SHELXTL-97 crystallographic software package.[1] During the refinement of compounds, several similar restraints were applied in obtain reasonable thermal parameters. All non-hydrogen atoms were refined with anisotropic thermal parameters. Data collection and refinement details are included in Table S1. Selected bond lengths and angles are given in Tables S2–S3. CCDC 1838628 and 1838629 contain the supplementary crystallographic data for this paper. These data are provided free of charge by The Cambridge Crystallographic Data Centre. The water molecule in compound **1** is disordered and could not be modeled properly, thus the SQUEEZE routine of PLATON was applied to remove the contributions to the scattering from the water molecule.

Table 1. The crystallographic data for compounds **1** and **2**.

Compound	**1**	**2**
formula	$C_{32}H_{29}N_5O_{16}Co_4$	$C_{39}H_{51}N_9O_{21}S_2Co_4$
M_r	975.26	1281.73
T (K)	293(2)	293(2)
Crystal system	triclinic	monoclinic
Space group	$P\bar{1}$	$P2_1/c$
a (Å)	13.262	16.075
b (Å)	18.495	18.529
c (Å)	22.258	17.861
α (deg)	89.11	90
β (deg)	76.32	90.47
γ (deg)	89.97	90
V (Å^3)	5303.915	5319.786
Z	4	4
ρ_{calcd}/g cm^{-3}	1.176	1.600
GOF	0.943	1.037
R_1 [$I > 2\sigma(I)$][a]	0.0788	0.0522
wR_2 [$I > 2\sigma(I)$][b]	0.2133	0.1258

[a] $R_1 = \sum(||F_0| - |F_c||)/\sum|F_0|$. [b] $wR_2 = [\sum w(|F_0|^2 - |F_c|^2)^2/\sum w(F_0^2)^2]^{1/2}$.

Table S2. Selected bond lengths (Å) and angles (°) for **1**.

Bond lengths [Å]			
Co(1)-O(1)	2.066(3)	Co(5)-O(3)	2.047(3)
Co(1)-O(9)	2.087(4)	Co(5)-O(23)	2.068(4)
Co(1)-O(11)	2.097(3)	Co(5)-O(6)	2.078(3)
Co(1)-O(2)	2.106(3)	Co(5)-O(19)	2.088(4)
Co(1)-N(1)	2.141(4)	Co(5)-N(6)	2.149(4)
Co(1)-O(8)	2.176(3)	Co(5)-O(21)	2.233(4)
Co(2)-O(2)	2.018(3)	Co(6)-O(4)	2.057(3)
Co(2)-O(13)	2.046(4)	Co(6)-O(5)	2.063(3)
Co(2)-O(10)	2.057(4)	Co(6)-O(3)	2.085(3)
Co(2)-O(15)	2.074(4)	Co(6)-O(26)	2.096(3)
Co(2)-N(2)	2.172(4)	Co(6)-N(7)	2.132(4)
Co(2)-O(8)	2.292(4)	Co(6)-O(21)	2.177(3)
Co(3)-O(2)	2.055(3)	Co(7)-O(4)	2.033(3)
Co(3)-O(18)	2.077(4)	Co(7)-O(22)	2.040(4)
Co(3)-O(12)	2.091(3)	Co(7)-O(27)	2.047(3)
Co(3)-O(1)	2.124(3)	Co(7)-N(8)	2.188(5)
Co(3)-O(14)	2.144(3)	Co(7)-N(10)#2	2.198(4)
Co(3)-N(9)#1	2.149(4)	Co(7)-O(24)	2.346(4)
Co(4)-O(1)	2.050(3)	Co(8)-O(3)	2.052(3)
Co(4)-O(17)	2.061(3)	Co(8)-O(28)	2.105(4)
Co(4)-O(7)	2.078(3)	Co(8)-N(3)#3	2.106(4)
Co(4)-N(4)	2.166(4)	Co(8)-O(4)	2.121(3)
Co(4)-N(5)	2.170(5)	Co(8)-O(25)	2.128(3)
Co(4)-O(14)	2.219(4)	Co(8)-O(24)	2.194(3)
Angles [deg]			
Co(4)-O(1)-Co(1)	130.56(16)	Co(5)-O(3)-Co(8)	131.68(16)
Co(4)-O(1)-Co(3)	97.86(12)	Co(5)-O(3)-Co(6)	97.36(13)
Co(1)-O(1)-Co(3)	90.54(13)	Co(8)-O(3)-Co(6)	92.68(13)
Co(2)-O(2)-Co(3)	128.81(15)	Co(7)-O(4)-Co(6)	129.31(16)
Co(2)-O(2)-Co(1)	101.85(13)	Co(7)-O(4)-Co(8)	101.45(13)
Co(3)-O(2)-Co(1)	91.36(14)	Co(6)-O(4)-Co(8)	91.49(14)
Co(1)-O(8)-Co(2)	91.52(12)	Co(6)-O(21)-Co(5)	89.43(13)
Co(3)-O(14)-Co(4)	92.30(13)	Co(8)-O(24)-Co(7)	90.16(12)

Symmetry Code: #1 x-1,y+1,z; #2 -x+1,-y,-z+2; #3 x,y-1,z.

Table S3. Selected bond lengths (Å) and angles (°) for **2**.

Bond lengths [Å]			
Co(1)-O(16)	2.017(3)	Co(3)-O(10)	1.996(3)
Co(1)-O(14)	2.020(4)	Co(3)-O(12)	2.013(3)
Co(1)-O(3)	2.098(3)	Co(3)-O(5)	2.118(4)
Co(1)-N(1)	2.122(4)	Co(3)-N(3)	2.136(4)
Co(1)-O(1)	2.174(3)	Co(3)-O(6)	2.190(3)
Co(1)-O(2)	2.221(3)	Co(3)-O(7)	2.223(3)
Co(2)-O(15)	2.068(3)	Co(4)-O(9)	2.064(3)
Co(2)-O(17)	2.082(4)	Co(4)-O(11)	2.069(3)
Co(2)-O(13)	2.089(3)	Co(4)-O(7)	2.107(3)
Co(2)-O(2)	2.120(3)	Co(4)-O(18)	2.110(5)
Co(2)-N(2)	2.134(4)	Co(4)-N(4)	2.138(4)
Co(2)-O(1)#1	2.172(3)	Co(4)-O(6)#2	2.160(3)
Angles [deg]			
Co(2)#1-O(1)-Co(1)	113.44(15)	Co(2)-O(2)-Co(1)	112.59(14)
Co(4)-O(7)-Co(3)	113.63(16)	Co(4)#2-O(6)-Co(3)	112.79(16)

Symmetry Code: #1 -x+2,-y,-z+1; #2 -x+1,-y,-z+2.

Table S4. BVS calculations for the Co ions in compounds **1** and **2**.

Compound	Atom	Co^{II}	Co^{III}
1	Co1	2.18	2.13
	Co2	2.11	2.14
	Co3	2.08	2.11
	Co4	2.14	2.18
	Co5	2.09	2.12
	Co6	2.14	2.18
	Co7	2.15	2.18
	Co8	2.12	2.15
2	Co1	2.14	2.18
	Co2	2.09	2.13
	Co3	2.12	2.16
	Co4	2.10	2.14

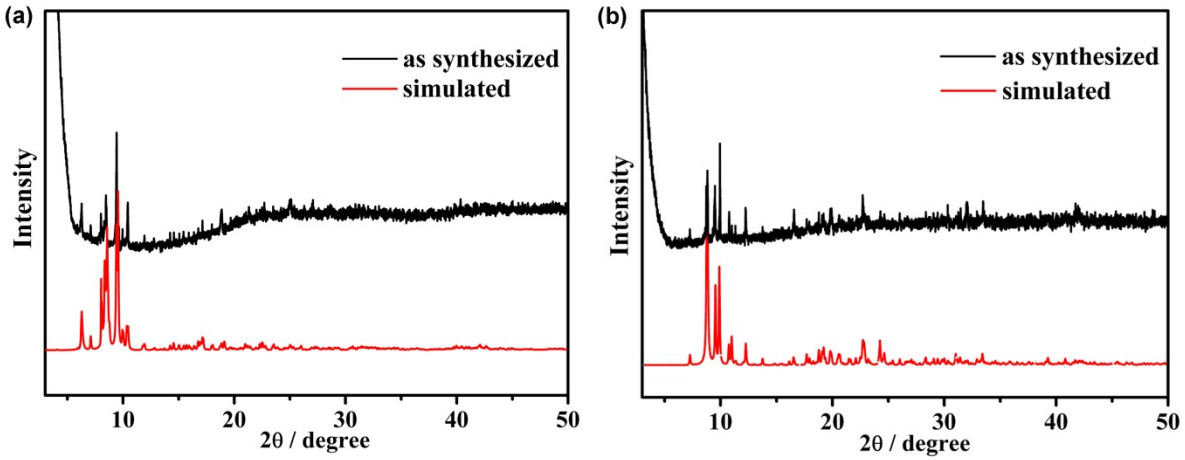

Figure S1. The PXRD patterns of **1** (a) and **2** (b).

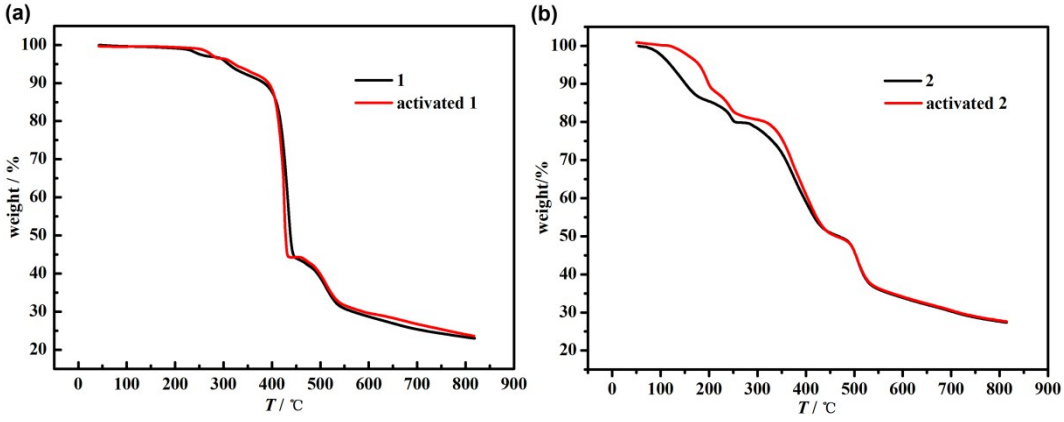

Figure S2. The TGA curves of **1** and activated **1** (a) and **2** and activated **2** (b).

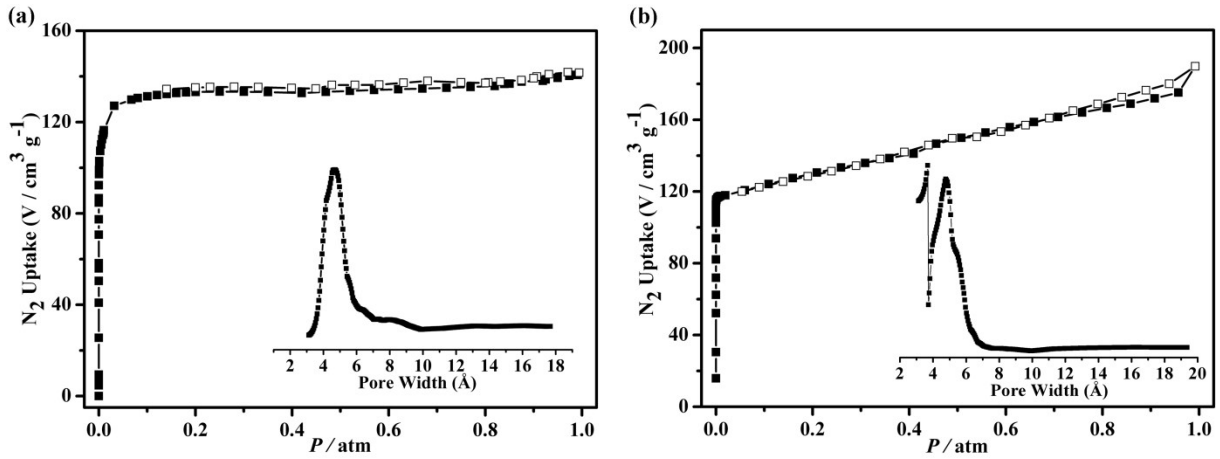

Figure S3. (a) N_2-adsorption isotherms at 77 K for **1** (a) and **2** (b). Filled and open symbols represent adsorption and desorption branches respectively. (Inset) Pore size distribution analyzed by HK methods.

CO_2/CH_4 Selectivity Prediction via Henry's law

The experimental isotherm data for pure CO_2 and CH_4 were fitted using a Single-site Langmuir model:

$$V_{ads}^{\ i} = \frac{V_{1i}K_{1i}P}{1 + K_1P}$$

Where V_{ads} is the total amount adsorbed in $cm^3\ g^{-1}$, P is the applied pressure in atm, V_i is the saturation capacity in $cm^3\ g^{-1}$, and K_i is the Langmuir affinity constant expressed in atm^{-1}. The fitting of the isotherm models was achieved by calculating the K_i and V_i parameters.

Selectivity at low coverage was calculated using the results of the single-site Langmuir fits of the experimental isotherms, by determining the Henry constants for each gas (Table S5) based on the equation:

$$H_i = \sum K_i V_i$$

The selectivity at zero pressure is then calculated with the relation:

$$S_{1,2} = \frac{H_1}{H_2}$$

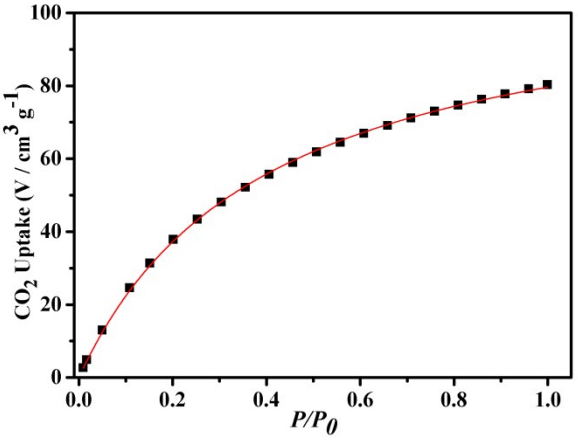

Figure S4. Adsorption isotherm of CO_2 recorded at 273 K for compound **1**. Solid line represents fitting curve using a single-site Langmuir model.

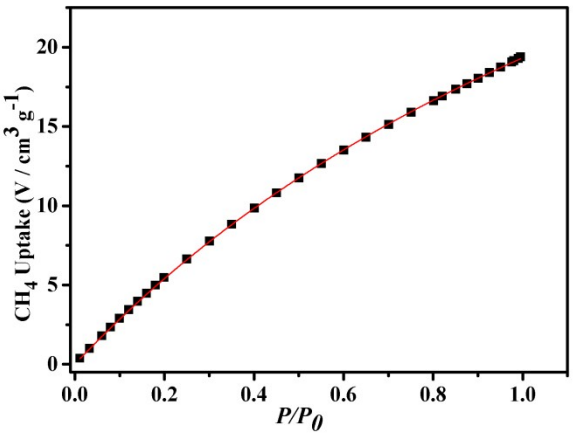

Figure S5. Adsorption isotherm of CH_4 recorded at 273 K for compound **1**. Solid line represents fitting curve using a single-site Langmuir model.

Table S5. Fit parameters for the CO_2 and CH_4 isotherms of compound **1** at 273 K and selectivity.

Compound 1	CO_2	CH_4	CO_2/CH_4 selectivity[c]
V_i[a]	111.39	54.37	9.3
K_i[b]	2.51	0.55	

[a] Saturation uptakes and [b] affinity constants estimated from a single Langmuir site model; [c] Selectivity estimated from the ratio of the Henry constant (= ratio of the initial slopes) at 273 K.

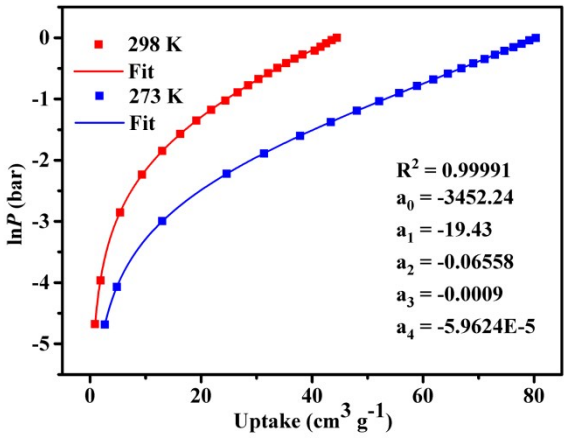

Figure S6. Virial analysis of CO_2 adsorption data at 273 K and 298 K. The solid lines show the virial equation fits for compound **1**.

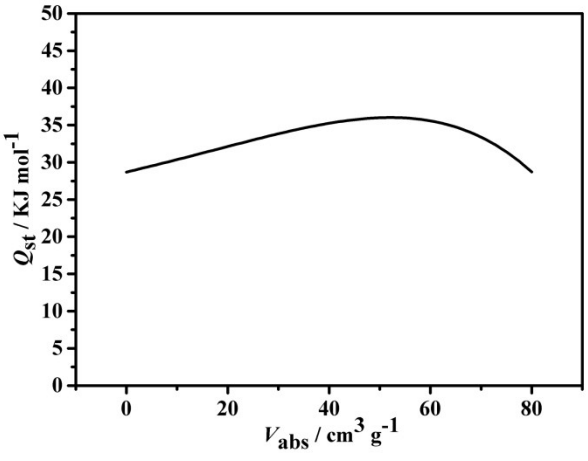

Figure S7. The coverage dependence of isosteric heat of CO_2 adsorption for **1** calculated from fits of their 273 K and 298 K isotherms.

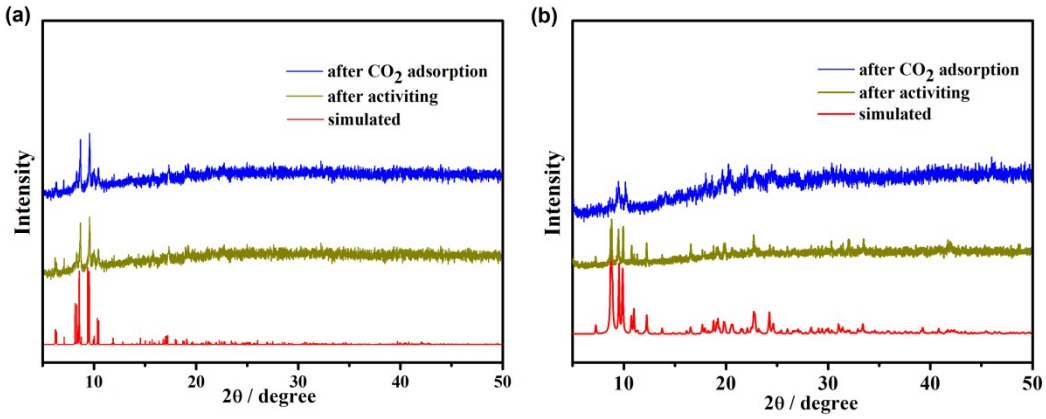

Figure S8. The PXRD patterns of **1** (a) and **2** (b) after an activation process and samples are measured with CO_2.

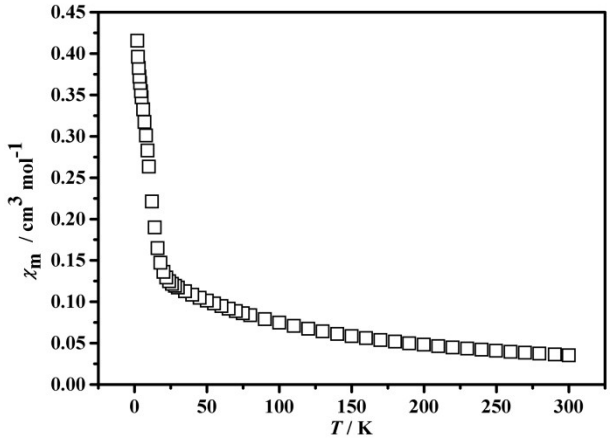

Figure S9. The temperature dependence of χ_m curve for **1**.

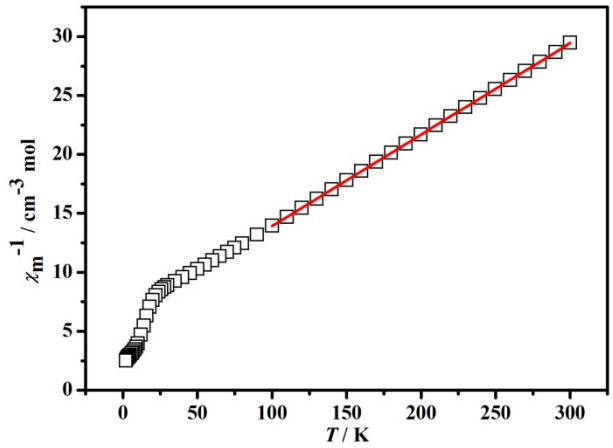

Figure S10. The temperature dependence of χ_m^{-1} for **1** under a static field of 1000 Oe.

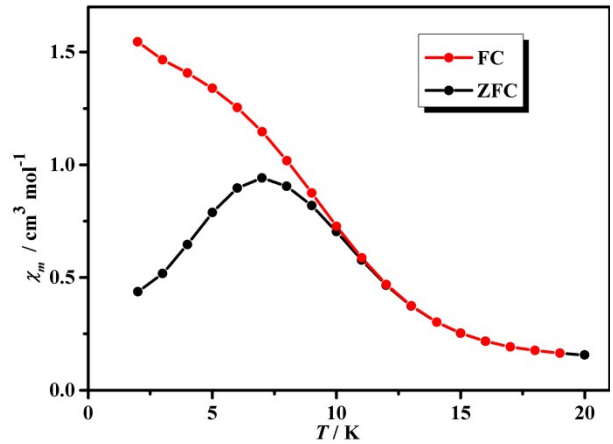

Figure S11. The FC and ZFC curves for **1** at an applied field of 100 Oe.

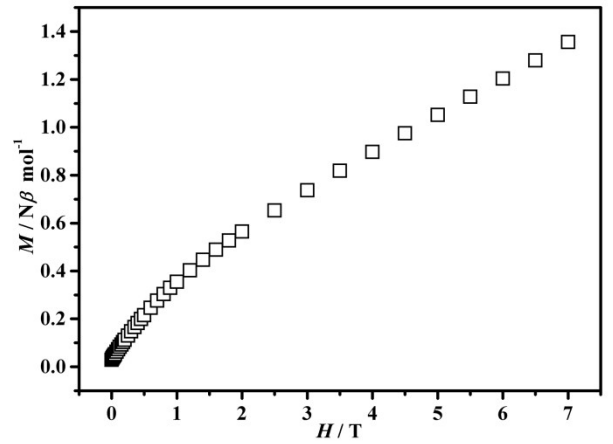

Figure S12. The field dependence of magnetization curve for **1**.

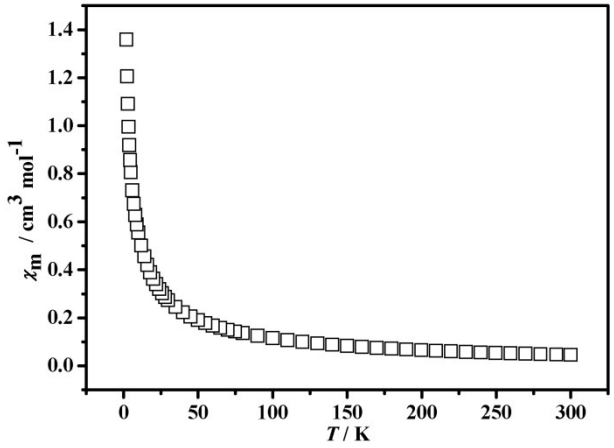

Figure S13. The temperature dependence of χ_m curve for **2**.

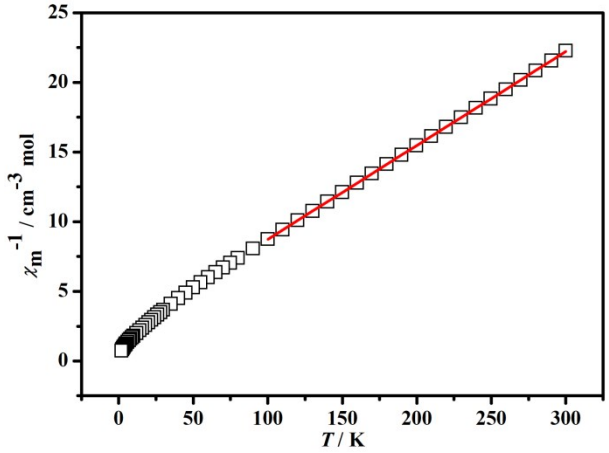

Figure S14. The temperature dependence of χ_m^{-1} for **2** under a static field of 1000 Oe.

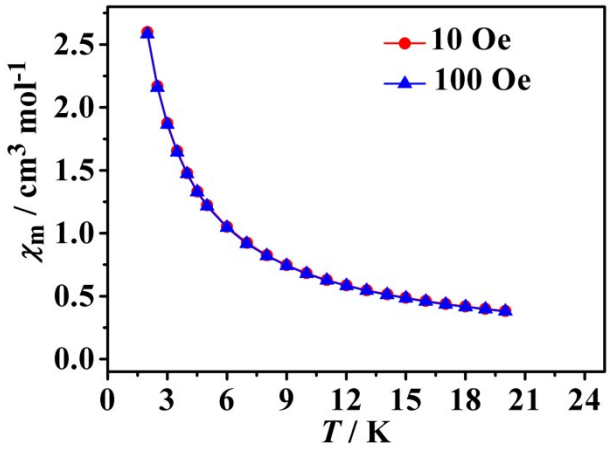

Figure S15. The temperature dependence of χ_m curve for **2** at the indicated applied field.

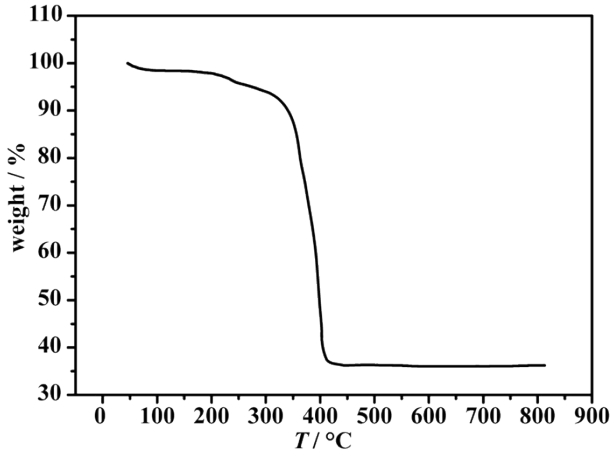

Figure S16. The TGA curve of **1** at air atmosphere.

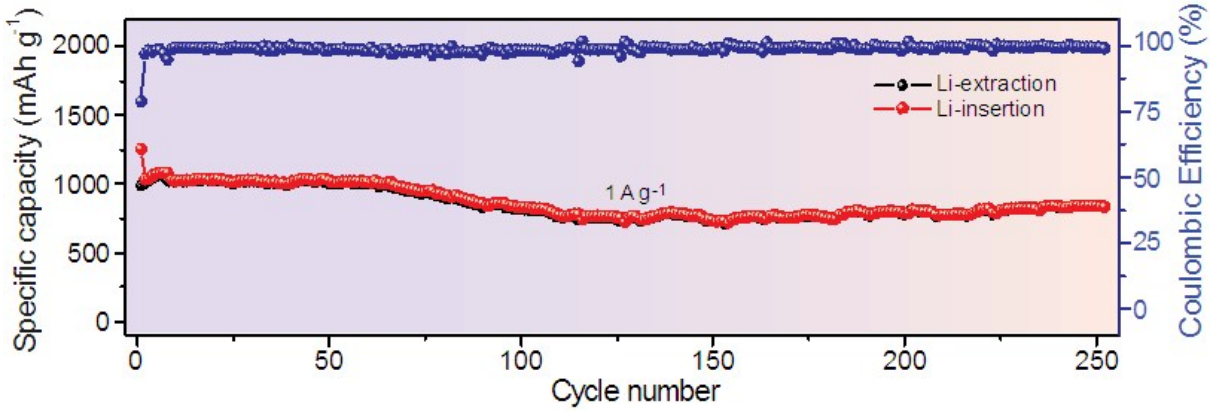

Figure S17. Cyclic performance of the Co_3O_4 electrode at 1 A g^{-1}.

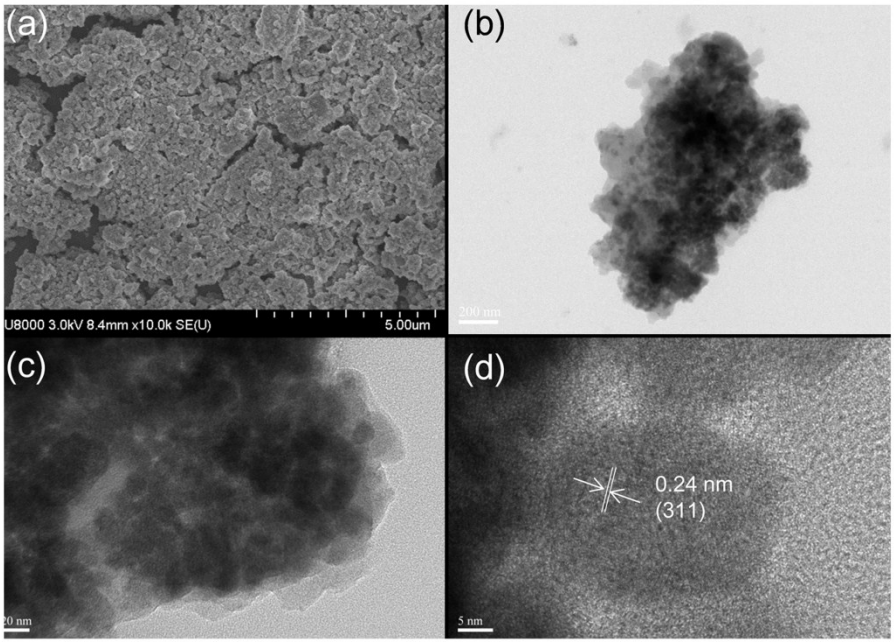

Figure S18. (a) SEM, (b, c) TEM and (d) HRTEM images of Co_3O_4 after cycles selected at different position, indicating the superior reversibility of Co_3O_4.

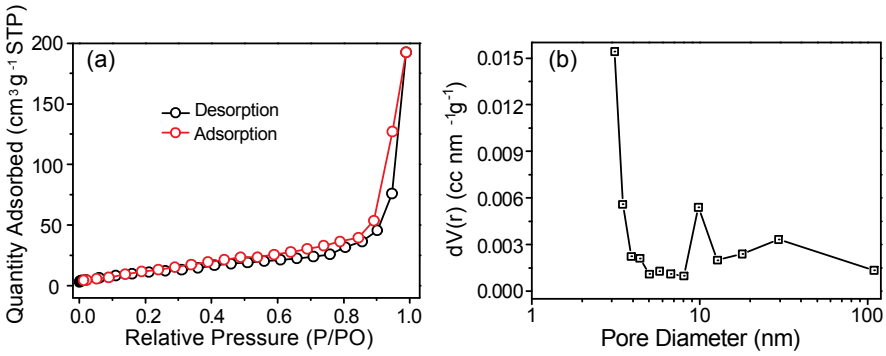

Figure S19. (a) Nitrogen adsorption–desorption isotherm and (b) the corresponding pore size distribution curve for Co_3O_4.

Table S6. Comparison of capacities of our Co_3O_4 electrode with Co_3O_4-based electrodes reported in the literatures.

Material	Capacity after 100 cycles	Rate performance	Initial CE	Ref.
Co_3O_4/nitrogen modified graphene	900 mAh g^{-1}@100 mA g^{-1}	800, 780, and 600 mAh g^{-1} @0.188, 0.313, and 0.625 A g^{-1}	77.3%	2
Co_3O_4 hollow-structured nanoparticles	770 mAh g^{-1}@100 mA g^{-1} after 50 cycles	850, 750, 600, and 450 mAh g^{-1} @0.1, 0.5, 1 and 2 A g^{-1}	79.4%	3
Co_3O_4/N-doped porous carbon hybrid	892 mAh g^{-1}@100 mA g^{-1}	1026, 947, 839, 627 and 560 mAh g^{-1} @1, 2, 5, 9 and 10 A g^{-1}	76.4%	4
Mesoporous nanostructured Co_3O_4	913 mAh g^{-1}@100 mA g^{-1}	800, 742.5, 442.1 and 100 mAh g^{-1} @0.4, 0.5, 1 and 2 A g^{-1}	68%	5
Peapod-like Co_3O_4@Carbon	862 mAh g^{-1}@100 mA g^{-1} after 60 cycles	700, 500, 453, and 408 mAh g^{-1} @0.2, 0.5, 1 and 5 A g^{-1}	~67%	6
Shale-like Co_3O_4	1045 mAh g^{-1}@200 mA g^{-1}	902.5, 784.1, 522.4, and 414.5 mAh g^{-1} @0.4, 1.6, 6.4, and 10 A g^{-1}	76.1%	7
Co_3O_4@Co_3O_4/N-C	1169 mAh g^{-1}@200 mA g^{-1}	1084.9, 986.6, 740.3, and 633.4 mAh g^{-1} @ 0.4, 1.6, 6.4 and 10 A g^{-1}	76.1%	8
Co_3O_4 nanospheres	1017 mAh g^{-1}@200 mA g^{-1}	1157.0, 1095.2, 1046.9, 991.3, 879.9, and 723.3 mAh g^{-1} @0.3, 1, 1.5, 2, 3 and 5 A g^{-1}	78.22%	**This work**

References

(1) (a) G. M. Sheldrick. SHELXL-97, Program for Crystal Structure Refinement, University of Göttingen, Göttingen (Germany), **1997**; (b) G. M. Sheldrick, SHELXS-97, Program for Crystal Structure Solution, University of Göttingen, Göttingen (Germany), **1997**; (c) G. M. Sheldrick. *Acta Crystallogr., Sect. A: Found. Crystallogr*. **2008**, *64*, 112−122.

(2) Lai, L.; Zhu, J.; Li, Z.; Yu, D. Y. W.; Jiang, S.; Cai, X.; Yan, Q.; Lam, Y. M.; Shen, Z.; Lin, J. *Nano Energy* **2014**, *3*, 134-143.

(3) Wang, D.; Yu, Y.; He, H.; Wang, J.; Zhou, W.; Abruña, H. D. *ACS Nano* **2015**, *9*, 1775-1781.

(4) Hou, Y.; Li, J.; Wen, Z.; Cui, S.; Yuan, C.; Chen, J. *Nano Energy* **2015**, *12*, 1-8.

(5) Li, C.; Chen, T.; Xu, W.; Lou, X.; Pan, L.; Chen, Q.; Hu, B. *J. Mater. Chem. A.* **2015**, *3*, 5585-5591.

(6) Gu, D.; Li, W.; Wang, F.; Bongard, H.; Spliethoff, B.; Schmidt, W.; Weidenthaler, C.; Xia, Y.; Zhao, D.; Schüth, F. *Angew. Chem. Int. Ed.* **2015**, *54*, 7060-7064.

(7) Li, H.-H.; Li, Z.-Y.; Wu, X.-L.; Zhang, L.-L.; Fan, C.-Y.; Wang, H.-F.; Li, X.-Y.; Wang, K.; Sun, H.-Z.; Zhang, J.-P. *J. Mater. Chem. A.* **2016**, *4*, 8242-8248.

(8) Li, H.-H.; Zhou, L.; Zhang, L.-L.; Fan, C.-Y.; Fan, H.-H.; Wu, X.-L.; Sun, H.-Z.; Zhang, J.-P. *ACS Energy Lett.* **2016**, *2*, 52-59.